IAP Annual Report 2004

ANNUAL REPORT 2004

INSTITUTE OF APPLIED PHYSICS

SWISS FEDERAL INSTITUTE OF TECHNOLOGY (ETH)

ZÜRICH

Mailing address:
ETH Zürich
Institut für Angewandte Physik
CH-8093 Zürich, Switzerland

Phone: +41-44-6332130
CH: 044-6332130
Telefax: +41-44-6331105
CH: 044-6331105

Prof. Dr. rer. nat. G. Kostorz

Phone: +41-44-6333399
e-mail "kostorz@iap.phys.ethz.ch"

INSTITUTE OF APPLIED PHYSICS ETH ZÜRICH

Guests 2004

Ph. D. students who are not employed by the institute

Daniel Abou-Ras (Laboratorium für Festkörperphysik)
Jay Padiyath (Laboratorium für Neutronenstreuung, Paul Scherrer Institut)
Dominik Rudmann (Laboratorium für Festkörperphysik) (until June 2004)
Dmitri S. Zimin (Laboratorium für Festkörperphysik) (until October 2004)

Staff 2004

Scientists (incl. employed Ph.D. students) Materials Physics

Dr. sc. nat. Myriam Haydee Aguirre (since June 2004)
Zsolt Geller, Dipl. Phys. ETH
Fabio Krogh, Dipl. Phys. Univ. La Sapienza, Rom, I
Dr. sc. techn. Peter Müllner (until June 2004)
Dr. Debashis Mukherji
Dr. phys. Stéphane Pecoraro (since October 2004)
Giancarlo Pigozzi, Dipl. Phys. Univ. Degli Studi, Milan, I (since January 2004)
Prof. Dr. rer. nat. Bernd Schönfeld
Alla S. Sologubenko, Dipl. Phys. Ukraine State Univ.
Christian Steiner, Dipl. Phys. ETH
Marije van der Klis, Dipl. Phys. Rijks Univ. Groningen

Scientists Electron Microscopy Center (EMEZ)

Dr. sc. nat. Myriam Haydee Aguirre (since June 2004)
Dr. sc. nat. Heinz Gross, Course Instructor
Dr. Andres Käch (BAL-TEC)
Dr. Nadejda B. Matsko
Dr. Martin Müller, Course Instructor

Technicians and Engineers
Materials Physics

Erwin Fischer
Josef Hecht
Ewald Vögele

Technicians and Engineers
EMEZ

Lilian Diener
Peter Tittmann
Peter Wägli (Lab. für Festkörperphysik)
Roland Wessicken (Lab. für Festkörperphysik)

Secretaries

Elisabeth Anner (80%) (until April 2004)
Ursula Huck (30%)
Helga Stettler (80%) (since April 2004)

The photo on the title page shows members and guests of the institute in February 2005.

INSTITUTE OF APPLIED PHYSICS ETH ZÜRICH

Teaching

(Academic year from October 2003 till September 2004)

Members of the institute participate in courses for physicists and materials engineers. During the last academic year, the following lectures were given (in German).

Winter Term 2003/2004

Materials physics I	with exercises	Prof. Dr. G. Kostorz
Materials physics with synchrotron radiation	with exercises	Prof. Dr. G. Kostorz Prof. Dr. B. Schönfeld Prof. Dr. J. F. van der Veen

Summer Term 2004

Materials physics II	with exercises	Prof. Dr. G. Kostorz
Principles of materials physics B	with exercises	Prof. Dr. G. Kostorz Prof. Dr. B. Schönfeld
Diffusion and phase transformations	with exercises	Prof. Dr. G. Kostorz Prof. Dr. B. Schönfeld
Cell biology V		Dr. H. Gross Dr. M. Müller Prof. Dr. Th. Wallimann

Three experimental setups for laboratory courses are available as experiments for third-year physics majors.

Laboratory work (term papers) continues to be available for third- and fourth-year physics and materials science students.

The institute participates in the organization of seminars in general physics, solid state physics and materials science. In the seminar on metal physics, current topics are discussed with visitors and local speakers.

Seminar speakers of the institute 2003/2004

Seminar on Metal Physics

Winter term 2003/2004

21 Oct. 03 Dr. R. Schäublin (CRPP-EPF, Lausanne, PSI, Villigen, CH):
TEM imaging of crystal nano defects.

28 Oct. 03 Dr. L. Lityńska (IMIM PAS, Kraków, PL):
Scandium in Al alloys.

04 Nov. 03 D. Abou-Ras:
Chemische Analyse mittels charakteristischer Röntgenstrahlung in der Rastertransmissionselektronenmikroskopie.

11 Nov. 03 Dr. F. Diologent (Laboratorium für Kristallographie, ETH Zürich, CH):
Creep behaviour of new generation nickel-base single crystal superalloys.

18 Nov. 03 M. van der Klis:
Das Spinglassystem Ag-Mn.

25 Nov. 03 Prof. G. Beaucage (University of Cincinnati):
In-situ study of the dynamics of nano-particle growth in a flame using synchrotron radiation.

09 Dec. 03 A.S. Sologubenko:
Polytypen und Phasenumwandlungen.

16 Dec. 03 Dr. D. Mukherji:
Nanostructured materials from superalloys.

06 Jan. 04 Prof. B. Schönfeld:
Verzerrungen in Legierungen.

13 Jan. 04 Ch. Steiner:
Die oberflächennahe Mikrostruktur von Pt-Rh.

20 Jan. 04 F. Krogh:
Bestimmung von Gleitsystemen in RuAl mittels Transmissionselektronen-mikroskopie.

27 Jan. 04 Z. Geller:
Neutronenkleinwinkelstreuung und Ni-reiches Ni-Re

03 Febr. 04 Dr. P. Müllner:
Strukturelle Instabilitäten und Martensitbildung

Summer term 2004

06 Apr. 04 D. Abou-Ras:
Diffusionsprozesse in Cu(In,Ga)Se_2-basierten Dünnschichtsolarzellen.

13 Apr. 04 G. Pigozzi:
Nanostructured materials from two-phase alloys.

20 Apr. 04 M. van der Klis:
Asymptotische Braggstreuung.

27 Apr. 04 F. Krogh:
<111>-Versetzungen in intermetallischen Verbindungen mit B2-Struktur.

04 May 04 Dr. P. Müllner (Boise State University, Boise, USA):
Magnetoplastizität von FePd.

18 May 04 Prof. G. Kostorz:
Phasenseparation in Nanodimensionen.

25 May 04 Prof. R. Kozubski (Jagellonian University Kraków, PL):
Superstructure refinement in bulk and nano-layered intermetallics: experiments and simulations.

01 June 04 Zs. Geller:
Thermisch diffuse Streuung an Legierungen.

08 June 04 D. Zimin:
Bragg mirrors for mid-infrared optoelectronic devices.

15 June 04 Prof. J. Rösler (Techn. Universität Braunschweig, D):
Superalloy research: from high-temperature alloys for power plants to nanoporous membrane materials.

22 June 04 Ch. Steiner:
Oberflächen und Ordnung.

29 June 04 Dr. C. Beeli (Laboratorium für Festkörperphysik, ETH Zürich, CH):
Elektronen-Holographie an Nanodrähten.

INSTITUTE OF APPLIED PHYSICS ETH ZÜRICH

Research

Since late 2002, the institute hosts the Electron Microscopy Center of the ETH Zürich (EMEZ) see page 2. The Center's activities are mostly covered in the reports of the twelve member laboratories. Electron Microscopy plays also an important role in Materials Physics, the traditional research area of the institute, as indicated below.

Research in Materials Physics

The institute's research concentrates on the study of the microstructure (incl. atomic resolution) of alloys and other materials in the bulk as well as at surfaces and interfaces, and of physical properties depending on microstructural features. Members of the institute are also actively involved in furthering the development of the methods serving these research interests.

In 2004, research funds were allocated by the Swiss Federal Institute of Technology Zürich itself and by the Swiss National Science Foundation.

Order and decomposition in alloys

Starting from a random solid solution, an alloy may show short- and long-range ordering and/or phase separation. Local atomic arrangements in crystalline alloys are studied by X-ray and neutron scattering as well as (conventional and high-resolution) transmission electron microscopy. The results are interpreted in terms of current theories of ordering and decomposition, accompanied by numerical studies of alloy behavior (e.g. Monte Carlo simulations). Current research concentrates on alloys based on Ni, Au and Pt.

Plasticity of alloys

Short-range order and precipitation affect the plastic deformation of alloys in various ways. During the past year, the deformation behavior of RuAl was studied as a function of temperature, and dislocation arrangements were analyzed by transmission electron microscopy. Phase transformations and magnetically induced deformation involving the motion of twins (magnetoplasticity) were studied in Mn-Al-C and Ni-Mn-Ga.

Interfaces

Studies on interfaces and the formation of twin domains in the metastable τ-phase of Al-Mn, a promising candidate for magnetoplasticity, were continued in 2004.

Methods of materials research

Special methods of X-ray and neutron scattering (small-angle and diffuse scattering), and of transmission electron microscopy are constantly advancing, and participation in the development of new methods and instruments, especially at synchrotron radiation and neutron scattering facilities, is required. Computer methods for the evaluation and simulation of materials behavior are also frequently used and continuously developed.

Major research topics active in the year 2004 are described below.
(Besides the head of the institute, the scientists given as contacts are available for further information.)

---

1. Short-range order and decomposition in alloys

Contacts: Prof. Dr. B. Schönfeld, Ch. Steiner, M.M.I.P. van der Klis, Zs. Geller
Collaborations: Swiss Light Source, PSI;
Neutron Scattering Laboratory, ETH Zürich and PSI

Elastic coherent diffuse scattering of X-rays and neutrons gives detailed information on the local atomic arrangements in alloys. Evaluation and interpretation of the contributions due to short-range order and static atomic displacements are well advanced. Equilibrium states are often established within reasonable periods of time only at high temperature. Owing to rapid kinetics, they cannot be frozen in by quenching to room temperature and thus, measurements of diffuse scattering are required at elevated temperature. Neutrons are then preferred to X-rays as they allow the inelastic thermal diffuse scattering to be separated experimentally. Nearly exclusively, the bulk structure of alloys has been investigated till now. In the past year, the near-surface microstructure of Pt-Rh was studied by grazing incidence diffraction using synchrotron radiation.

The bulk microstructure of single-crystalline Pt-47 at.% Rh aged at 650°C and investigated by small-angle neutron scattering and wide-angle X-ray scattering at room temperature, shows modulations in short-range order scattering (the deviations from the monotonic Laue scattering) that are small. Weak intensity maxima are observed at 1 ½ 0 [1]. The sign sequence of the leading Warren-Cowley short-range order parameters and a configurational analysis of nearest-neighbor configurations support the structure “40” as ground-state structure. The main feature in the coherent diffuse scattering is a strong modulation due to size-effect scattering, unexpected for the small atomic size difference of 3% between Pt and Rh.

Atom-probe field-ion microscopy investigations of Pt-Rh showed a slight tendency for local decomposition [2]. Calculated segregation profiles [3] revealed a high Pt concentration in the surface layer, a high Rh concentration in the second layer, and about the bulk composition for the subsequent layers. Surface-sensitive studies on Pt-75 at.% Rh at room temperature performed by Hebenstreit et al. [4] showed local order for the (111) and (100) surfaces. A transformation to a missing-row reconstruction was found for the (110) surface above 750°C.

For the present near-surface microstructural studies, a slice of Pt-47 at.% Rh with a [110] surface normal was prepared, with a final polish of 0.04 μm Al_2O_3. Samples were transferred to the Materials Science Beamline 4S (surface diffraction, SLS) in a portable UHV chamber. Sputtering with 1.5 keV Ar ions at 500°C and annealing at 850°C were repeatedly done before taking data. Horizontal mounting of the sample was chosen to benefit from the better vertical focusing of the incoming beam (Fig. 1.1).

Fig. 1.1 Portable UHV chamber mounted in the horizontal set-up on the (2+3) surface diffractometer at the Materials Science Beamline at SLS.

Diffuse scattering was taken at 730°C with the glancing angles of the incoming and scattered beam both set to 0.33° (the critical angle α_c is 0.45° for photons of 9.659 keV). About 700 positions were measured with scattering vectors between 0.1 to 3.4 reciprocal-lattice units. The background was flat, with 50 counts per 200 s. The diffuse scattering had about 200 to 1000 counts per 200 s.

The collected data were corrected for the scattering geometry, polarization factor and surface misorientation (better than 0.05°), using symmetry equivalent positions and employing the distorted-wave Born approximation. The Debye-Waller factor $\exp[-2B(\sin\theta/\lambda)^2]$, with $B = 1.11 \times 10^{-2}$ nm^2, was estimated using the elastic constants of the bulk material [1] at room temperature and extrapolating them to elevated temperatures (see Dereli et al. [5]). Diffuse scattering was calibrated using the calculated thermal diffuse scattering around Bragg reflections.

Fig. 1.2 shows the total diffuse scattering in Laue units within the (110) plane. Thermal diffuse scattering is seen as the dominating contribution. No diffuse maxima are observed neither close to the direct beam nor between the Bragg reflections. The enhanced intensities at 100-type positions come from the crystal truncation rods [6]. No (1 × 3) missing-row reconstruction is observed, in contrast to results of investigations at room temperature [6]. After subtracting Compton scattering and thermal diffuse scattering, the elastic diffuse scattering was fitted to a set of Warren-Cowley short-range order parameters and linear and quadratic displacement parameters. No species-dependence of the displacement parameters is considered in this fitting (so called Borie-Sparks evaluation). The recalculated short-range order scattering and also the size-effect scattering look similar to the results from the bulk (Fig. 1.3); (i) short-range order scattering shows diffuse maxima at 1 ½ 0 positions and (ii) size-effect scattering shows an asymmetry across the Bragg reflections. Further investigations are under way to reveal the near-surface microstructure for other types of surface orientation.

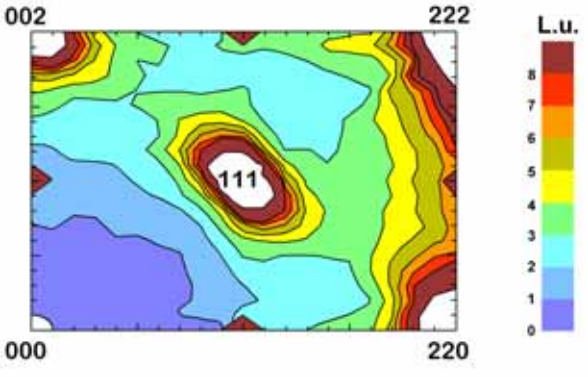

Fig. 1.2 Diffuse scattering in the (110) plane from the near-surface microstructure in Laue units (L.u., one Laue unit = elastic diffuse scattering of a random solid solution of the same average composition). Isointensity lines around the four Bragg reflections larger than 9 L.u. are not shown.

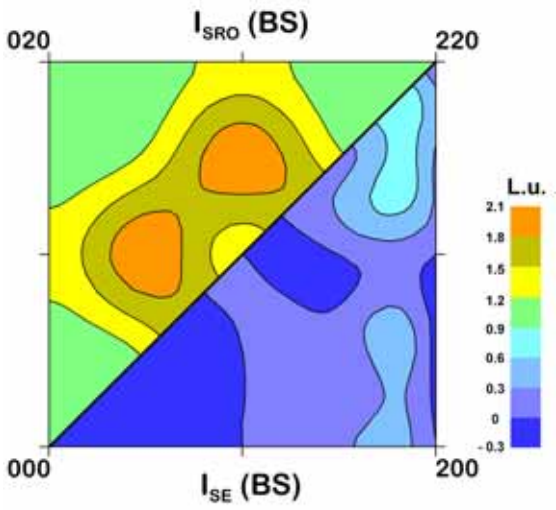

Fig. 1.3 Short-range order scattering and size effect scattering (in Laue units) in the (100)-plane recalculated from the fitted parameters of the (110) near-surface microstructure.

References

1. Ch. Steiner, B. Schönfeld, M. J. Portmann, M. Kompatscher, G. Kostorz, A. Mazuelas, T. Metzger, J. Kohlbrecher, B. Demé, Phys. Rev. B, in print.
2. T. T. Tsong, S. B. McLane, Jr., M. Ahmad, C. S. Wu, J. Appl. Phys. **53** (1982) 4180.
3. V. Drchal, A. Pasturel, R. Monier, J. Kudrnovský, P. Weinberger, Comput. Mater. Sci. **15** (1999) 144.
4. E. L. D. Hebenstreit, W. Hebenstreit, M. Schmid, P. Varga, Surf. Sci. **441** (1999) 441.
5. G. Dereli, T. Cagin, M. Uludogan, M. Tomak, Phil. Mag. Lett. **75** (1975) 209.
6. R. Koller, Y. Gauthier, C. Klein, M. De Santis, M. Schmid, P. Varga, Surf. Sci. **530** (2003) 121.
7. I. K. Robinson, Phys. Rev. B **33** (1986) 3830.

2. Coherent formation of plate-like τ in MnAl-C

Contacts: A. S. Sologubenko
Collaborations: Boise State University, Boise, Idaho, USA

The metastable ferromagnetic τ-phase ($L1_0$ structure) possesses attractive magnetic properties and is used in permanent magnets. The magnetic properties of the τ-phase depend on the microstructure. With a high density of twins, large uniaxial magnetic anisotropy, strong magneto-mechanical coupling, and sensitivity of the microstructure to alloy processing, τ-MnAl-C meets the conditions for a large magnetoplastic response.

The τ-phase appears in two morphological modifications: flower-like τ and plate-like τ. Both modifications form from the supercooled high-temperature ε-phase (A3 structure) during isothermal annealing. They result from two different transformation mechanisms and therefore have different microstructures. Each modification has its own composition-temperature preponderance region in the Mn-Al phase diagram [1]. Flower-like τ results from the composition-invariant, diffusion-controlled massive transformation mode that yields no specific orientation relationship between the ε-matrix and the product τ-phase [2]. Flower-like τ nucleates mainly at the grain boundaries and impurities in the lattice and propagates in the matrix by migration of coherent or partially coherent interfaces yielding the flower-like morphology. Plate-like τ forms by a displacive transformation in a step-like mode [3]. The plate-like τ-phase retains a specific orientation relationship $(0001)_\varepsilon // (111)_\tau$, $[11\bar{2}0]_\varepsilon // [\bar{1}10]_\tau$ to the matrix ε-phase across the intermediate steps of the transformation and appears in the form of piles of plates [1]. The coherency is transmitted by the intermediate orthorhombic ε′-phase (B19 structure) [4].

Three orientation variants of the ordered ε′-phase form coherently in the order reaction $\varepsilon \rightarrow \varepsilon'$. The nucleation sites of the plate-like τ-phase are considered to be the domain boundaries of the orientation variants of ε′ [3]. The nuclei are stacking-faults (SFs) extended across a domain parallel to the basal planes of the parent ε-phase and pinned at the domain boundary by Shockley partial dislocations. The SFs arise within a domain at some definite stage of the ε′ growth and coarsening. It has been suggested [3] that shear occurs when lattice coherency at ε/ε′ or $\varepsilon'_i/\varepsilon'_j$ (i, j = 1, 2, 3) interfaces cannot be maintained any longer. Lattice mismatch arrives at the critical value when the critical size of the ε′-domains is reached and/or when the degree of order in ε′ progresses to a certain value. At this stage, the ABAB stacking sequence of the B19 lattice starts to be distorted. Shear is accompanied by twinning. The SFs order themselves to reduce the transformation stresses carried by the partial dislocations involved in the transformation. The τ-phase appears as a set of twinned lamellae when the ordered arrays of stacking-faults (polytypes) within single ε′-domains overcome the boundaries and propagate into neighboring domains. Each orientation variant of ε′ produces two twin-related orientation variants of the plate-like τ-phase [3].

In contrast to the massive transformation mechanism that always yields polycrystalline τ, the displacive transformation mode can be controlled to produce a single crystal or a polysynthetically twinned crystal [1, 4]. This option is a necessity for fully exploiting the potential of magnetoplasticity.

The kinetics of evolution of the orthorhombic ε′-phase in three orientation variants control the nucleation of plate-like τ. To study the ε → ε′ ordering process, transmission electron microscopy (TEM) and X-ray diffraction studies were performed with two crystals of compositions Mn - 39.2 at.% Al - 0.8 at.% C and Mn - 41.2 at.% Al - 0.8 at.% C (carbon is added to slow down the kinetics).

TEM studies of Mn - 39.2 at.% Al - 0.8 at.% C annealed at 300°C show that at this stage of the transformation, the matrix ε is very likely entirely transformed to the ε′-phase. Figure 2.1a is a high-resolution transmission electron microscopy (HRTEM) image taken in $[0002]\varepsilon \parallel [200]\varepsilon'$ zone axis. The patch-work pattern in the image reveals the simultaneous occurrence of three orientation variants of the orthorhombic ε′-phase. The long-range ordered ε′-domains are completely coherent. The corresponding diffraction pattern taken from a much larger area is shown in Fig. 2.1b. The superlattice reflections of all three ε'_i variants are present. A dense net of antiphase boundaries (APBs) is found in the TEM foil. The APBs terminate at a domain boundary or extend across a boundary into a neighboring domain.

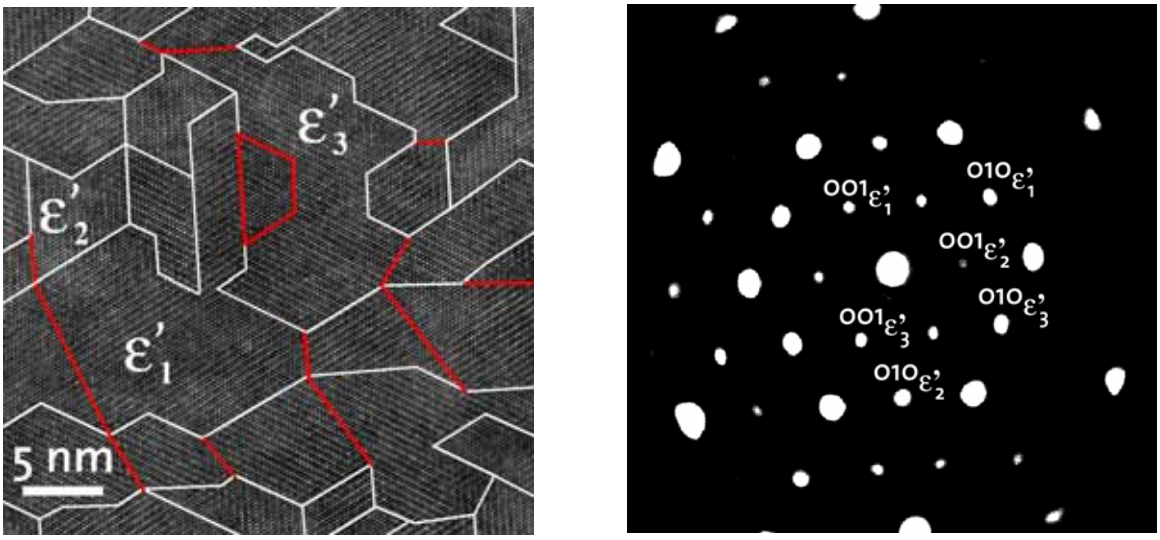

(a) (b)

Fig. 2.1 (a) HRTEM image taken in [0002]ε zone axis from Mn – 39.2 at.% Al – 0.8 at.% C annealed at 300°C for 21 h. The patch-work pattern of domains of the three ε′-orientation variants is outlined. White lines mark the ε′-domain interfaces. Red lines correspond to antiphase boundaries in ε′. Domain interfaces are coherent. (b) Diffraction pattern taken in [0002]ε zone axis from a much larger area. The superlattice reflections of all three ε′-variants are present.

Figure 2.2a shows a bright-field image taken close to the $[0002]\varepsilon \parallel [200]\varepsilon'$ zone axis of the same crystal. The strain-field contrast reflects the symmetry of the ε′-domain arrangement morphology. Our observations confirm the computer simulations performed by Wen et al. [5] on the formation and temporal evolution of domain structures during the hexagonal → orthorhombic transition. According to these results [5], the ε → ε′ reaction can be split into two steps. Initially, nucleation and growth of the ε′-domains occurs within ε, and coarsening of the ε′-domains follows after the matrix has been fully transformed to ε′. The elastic interactions between domains result in the formation of specific domain arrangements with minimized av-

erage elastic strain energy [6]. Shear occurs when the strain energy cannot be reduced further by domain rearrangement, and stacking faults appear. The intersections of APBs with ε′-domain boundaries are assumed to be nucleation sites for the stacking faults (see Fig. 2.2b, arrow). Along the transformation path, the stacking-faults rearrange within the ε′-domains to form thin twinned plates of polytypes (P). Eventually, the polytypes overcome the ε′-domain boundaries and propagate into the neighboring domains [3].

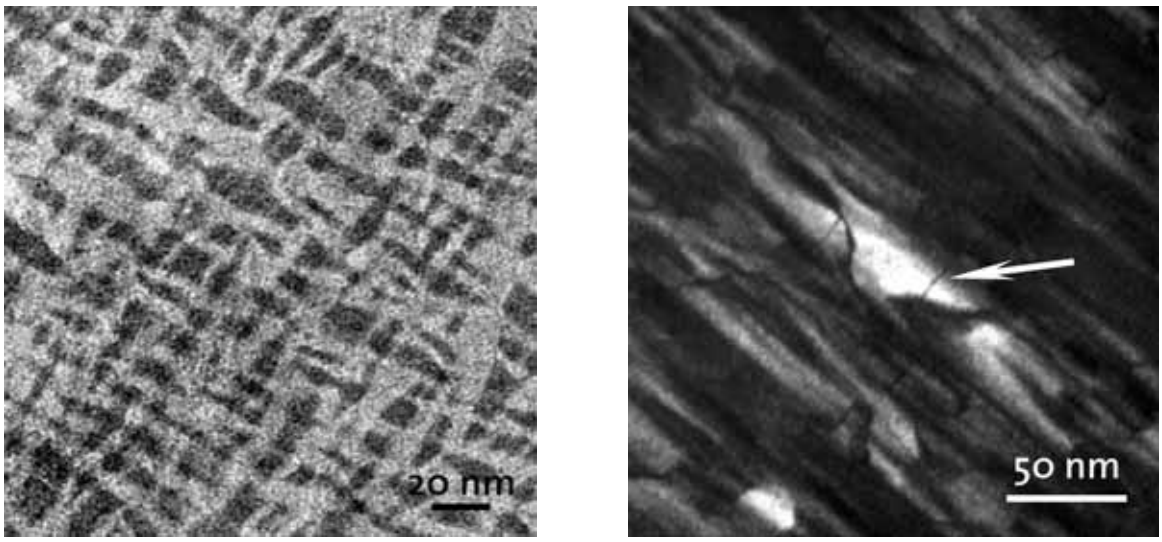

(a) (b)

Fig. 2.2 (a) Bright-field image taken about 2° off the [0002]ε zone axis of Mn – 39.2 at.% Al – 0.8 at.% C annealed at 300°C for 21 h. The distribution of dark regions demonstrates the strain-field symmetry in the lattice. (b) Dark-field image taken in $[11\bar{2}0]\varepsilon \parallel [010]\varepsilon'_1$ zone axis in two-beam condition with $201\varepsilon'_1$ as the second strong reflection. The bright elongated regions correspond to the ε'_1-domain regions in the lattice. The nearly straight lines crossing the image diagonally show the domain boundaries. The black straight lines within ε'_1-domains (arrow) are the stacking-faults terminating at both the wavy dark-imaged APBs within domains and the domain boundaries.

Reordering of neighboring ε′-domains must occur for the polytypes to propagate. X-ray measurements of the degree of order η of ε′ at different stages of ordering were performed on Mn – 41.2 at.% Al – 0.8 at.% C. The measurements were made on a sample (*i*) initially unannealed, (*ii*) annealed at 300°C for 5 h, and, (*iii*) additionally annealed at 300°C for 10 h. Results are shown in Table 1. Metallographic studies of the crystal after each X-ray measurement revealed that the plate-like τ-phase had appeared during the last annealing (300°C, 5+10 h).

Table 1 Order parameter η of Mn – 41.2 at.% Al – 0.8 at.% C after various heat treatments.

State of annealing	η
unannealed	0.10 (2)
300°C, 5 h	0.27 (3)
300°C, 5+10h	0.31 (5)

It is concluded that the matrix ε is not present when the plate-like τ appears. Thus, the ε → plate-like τ formation process is a discontinuous sequence of coherent phase-transformation steps: ε → ε′ → ε′ + SFs → ε′ + P → τ. The ε′-domains limit the spatial extension of the transformation field until the very last step. The lattice misfit between the domains of different ε′-orientation variants increases during ordering and domain growth. Coherency stresses at the domain interfaces rise until shear occurs to release the stresses. The critical size of the domains is ≤ 50 nm [3], and the critical value of the degree of order is about 0.30. Assuming that the plate-like τ inherits to some extent the degree of order in ε′, it is concluded that the plate-like τ is, at least initially, not completely ordered.

References

1. A. S. Sologubenko, P. Müllner, H. Heinrich, M. Wollgarten, G. Kostorz, J. Phys. IV France **112** (2203) 1071.
2. C. Yanar, J.M. K. Wiezorek, V. Radmilovich, W. A. Soffa, Metall. Mater. Trans. A**33** (2002) 1.
3. A. S. Sologubenko, P. Müllner, H. Heinrich, G. Kostorz, Z. Metallkd. **95** (2004) 6.
4. S. Kojima, T. Ohtani, N. Kato, K. Kojima, Y. Sakamoto, I. Konno, M. Tsukahara, T. Kubo, AIP Conf. Proc. **24** (1975) 768.
5. Y. H. Wen, Y. Wang, L. Q. Chen, Phil. Mag. A **80** (2000) 1967.
6. L.-Q. Chen, Y. Wang, A. G. Khachaturyan, Phil. Mag. Lett. **65** (1992) 15.

---

3. Nano-structured materials from two-phase metallic alloys

Contacts: Dr. D. Mukherji, G. Pigozzi
Collaborations: Institute for Physical Hightechnology, Jena, Germany
FRM-II, Technical University Munich, Garching, Germany
Neutron Scattering Laboratory, ETH Zürich and PSI
Technical University Braunschweig, Braunschweig, Germany

A variety of physical and chemical methods have been employed to synthesize nanostructured materials from semiconductors, metals, oxides and other ceramics [1]. Recently, a new method has been developed to produce nanostructured material of metallic and intermetallic type from bulk metallic alloys [2]. With this technique it is quite possible to produce a large variety of nano-structured materials - e.g. nano-particles [2] or nano-porous structures [3] - starting from the same bulk alloy. In a metallic alloy containing precipitates of a second phase, it is possible to control the precipitate morphology and size by heat treatment and other processing parameters as, e.g., in thermo-mechanical processing, to form different nano-scale features in the microstructure of the bulk material. It is also possible to isolate these nano-sized features from the bulk by removing the second phase. This is achieved by selective phase dissolution, for example by electro-chemical processing [2, 3]. In this way, it is possible to isolate nano-particles of complex compositions or produce other functional materials like a

unique nano-porous metallic membrane [3]. The process is very flexible and can be applied to different metallic systems. It essentially requires two steps, (*i*) establishing the nano-structure in bulk material, (*ii*) separating the nano-structure from the bulk.

In principle, most metallic alloys containing two phases (one phase often dispersed) may be used as the starting material. In systems where the precipitates are coherently embedded in the matrix (e.g. Ni-Al, Ni-Si, Fe-Al-Ni, etc.), the morphology and the size of the precipitate phase are controlled to a large extent by the lattice-parameter misfit between the matrix and the precipitate phase. A vast literature exists on the nucleation and growth kinetics of such precipitates, especially aluminides and silicides in different alloy systems (see, e.g., Ref. [4]). Most of these precipitates can be controlled to ultra-fine sizes (on the nano-scale) by suitable heat treatment of the bulk alloy. Non-equilibrium processes like rapid quenching or severe plastic deformation may also be used to obtain nano-size precipitates.

The most important processing step for the fabrication of nano-structured material by the new process presented here is the selective phase dissolution. This is possible by electrochemical dissolution. Selective phase dissolution was performed electro-chemically at preselected current density (galvanostatic method) or at preselected potential (potentiostatic method). The sample is chosen as the working electrode (anode), and Pt may be used as the counter electrode (cathode) in the electrolytic cell. For example, from a Ni-base superalloy containing nano-size precipitates, a loose Ni_3Al-type powder is thus obtained in the case of matrix dissolution (Fig. 3.1).

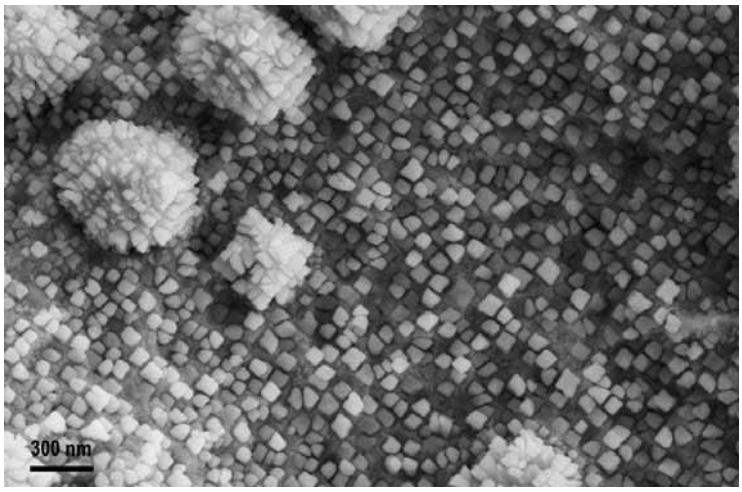

Fig. 3.1 Nano-particles of Ni_3Al type, sticking on the surface of the specimen after extraction from a Ni-base superalloy. The particle diameter is about 80 nm. Some clustering of loose particles is visible.

Fig. 3.2 shows the precipitate microstructure of a binary Ni-14.5 at.% Si alloy after isothermal heat treatment at 600°C for 24 h. The precipitate particles (Ni_3Si) are spherical and are well dispersed in the matrix (Fig. 3.2a). Fig. 3.2b shows a high-resolution transmission electron micrograph of an isolated particle after it was extracted from the bulk. The particle was imaged along the [001] zone axis, and the image shows that the lattice spacings at the core of the particle and near its surface are quite similar. Further, the particle surface is relatively clean, as evident from the lattice image which extends up to the surface layer. The lattice parameter of a sample containing Ni_3Si particles ($L1_2$ structure) of ~ 20 nm diameter was measured by

X-ray diffraction and found to be 0.3511(1) nm. This value does not significantly deviate from 0.351 nm, reported for bulk Ni_3Si samples [5].

Nano-size particles obtained by this process may, for example, be used for the fabrication of composites with bulk metallic glasses as the matrix.

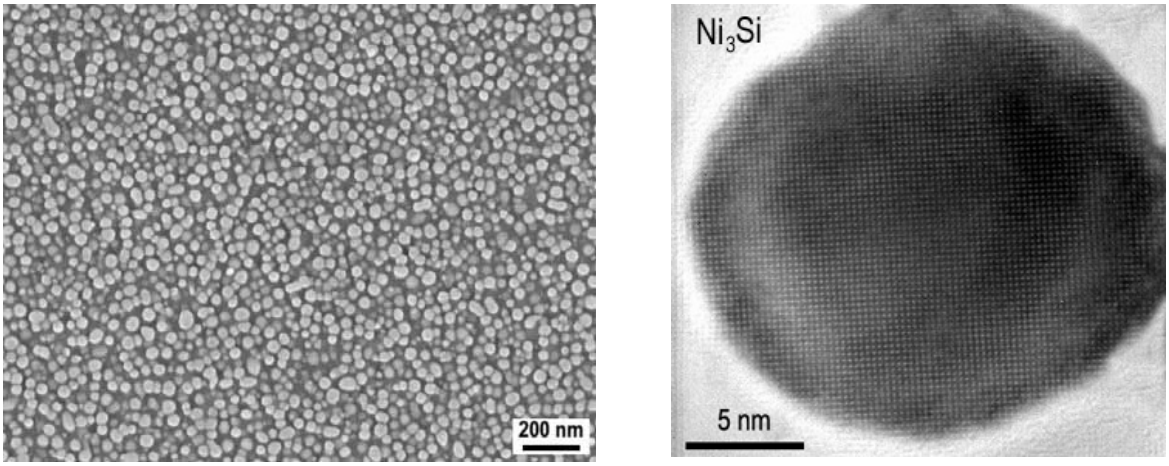

(a) (b)

Fig. 3.2 (a) Microstructure of Ni_3Si precipitates in Ni-14.5 at.% Si alloy, (b) high-resolution TEM image of an extracted Ni_3Si particle about 20 nm in diameter.

References

1. H. S. Nalwa (Ed.), "Handbook of Nanostructured Materials and Nanotechnology: Synthesis and Processing", Vol. 1, Academic Press, San Diego, USA, 2000.
2. D. Mukherji, R. Müller, R. Gilles, P. Strunz, J. Rösler, G. Kostorz, Nanotechnology **15** (2004) 648.
3. J. Rösler, D. Mukherji, Adv. Eng. Mater. **5** (2003) 916.
4. M. Doi, Prog. Mater. Sci. **40 (**1996) 79.
5. S. Ochiai, Y. Oya, T. Suzuki, Bull. P.M.E. (T.I.T) **52 (**1983) 1.

4. Investigation of In_xS_y buffer layers deposited by different techniques for $Cu(In,Ga)Se_2$ thin-film solar cells

Contacts: D. Abou-Ras, D. Mukherji
Collaborations: Thin Film Physics Group of the Lab. for Solid State Physics, ETH Zürich
University of Stuttgart, Germany
Center for Solar Energy and Hydrogen Research (ZSW), Stuttgart, Germany

Polycrystalline thin-film solar cells based on $Cu(In,Ga)Se_2$ (CIGS) are important for terrestrial applications because of their high efficiency, long-term stable performance and potential for low-cost production. Record efficiencies of more than 19% have been achieved [1]. The solar cells consist of a substrate, a back-contact layer, the p-type CIGS absorber, an n-type buffer layer, and a front contact which is usually a combination of i:ZnO and ZnO:Al.

As for the buffer layer, different semiconductor compounds with n-type conductivity and band gaps between 2.0 and 3.6 eV have been applied. However, CdS remains the most widely investigated buffer layer, as it has continuously yielded high-efficiency cells. CdS buffer layers are generally grown by chemical bath deposition. However, because of the relatively low CdS bandgap of ca. 2.4 eV and also for environmental reasons, alternative buffer layer materials are being sought. A very promising material is In_2S_3 since solar cells consisting of an In_2S_3 buffer layer grown by atomic layer deposition (ALD) recently yielded more than 16% efficiency [2] on small areas.

However, the up-scaling of the ALD process for industrial production of In_2S_3 buffer layers causes difficulties. Thus, In_2S_3 buffer layers are also produced by physical vapor deposition (PVD) and sputtering. Recently, 14.8% efficiency has been achieved applying PVD-In_xS_y buffer layers [3] (the notation "In_xS_y" is used, since these layers are produced by evaporation of an In_2S_3 compound, but they consist of various In-S phases).

The interface between the p-type CIGS absorber and the n-type In_2S_3 is the most important one in the solar cell since there, the p-n junction is formed. Structural and chemical investigations of CIGS/In_2S_3 interfaces provide valuable information on the junction formation, complementary to the electrical data. Thus, ALD-, PVD- and sputtered In_xS_y layers and their interfaces with CIGS have been studied by means of bright-field and high-resolution transmission electron microscopy, electron diffraction, and energy-dispersive X-ray spectrometry.

For CIGS solar cells with ALD-In_2S_3 buffer layers, the efficiencies decrease with increasing substrate temperature for substrate temperatures larger than 210-220°C. A comparison of high-resolution transmission electron micrographs from CIGS/ALD-In_2S_3 interfaces with the In_2S_3 layers deposited at 210°C and 240°C substrate temperatures (Fig. 4.1) shows an abrupt interface and good lattice match between the CIGS and the In_2S_3 layer for the 210°C sample.

In contrast, at the 240°C-In_2S_3/CIGS interface, an interfacial layer is revealed between In_2S_3 and CIGS. The nature of this layer cannot be identified by electron diffraction on this interface, since the interfacial layer has a thickness of only 10-15 nm, thus, the excitation volume is too small.

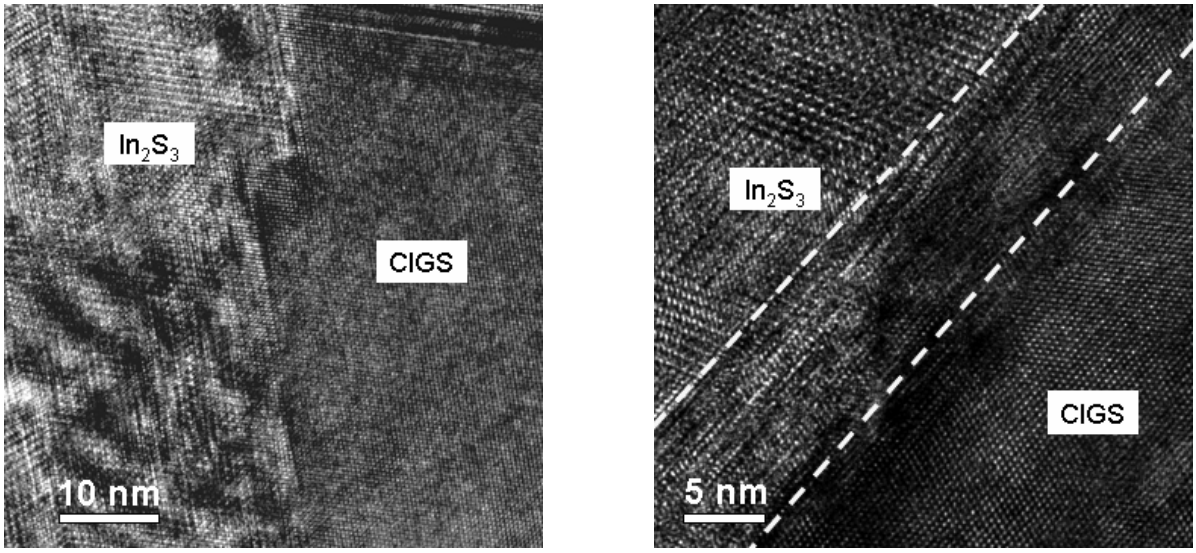

(a) (b)

Fig. 4.1 High-resolution transmission electron micrograph from the interface of CIGS with ALD-In_2S_3 layers grown at (a) 210°C and (b) 240°C. While there is a good lattice match between In_2S_3 and CIGS for the 210°C sample, an interfacial layer is revealed between CIGS and In_2S_3 in the 240°C sample.

Measurements on interfaces of CIGS with PVD-In_xS_y and sputtered In_2S_3 layers, both deposited at 300°C substrate temperature, show similar interfacial layers with larger thicknesses, and the phase of these layers has been identified as $CuIn_5S_8$ (Fig. 4.2).

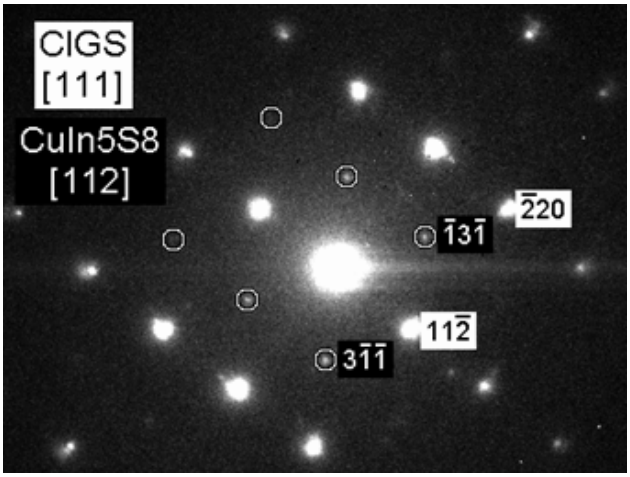

Fig. 4.2 Electron diffraction pattern from an interface between CIGS and a sputtered-In_2S_3 layer deposited at about 300°C substrate temperature.

It is assumed that for all CIGS/In_xS_y interfaces with the In_xS_y layer deposited at substrate temperatures larger than about 230-250°C, $CuIn_5S_8$ forms as an interfacial layer between CIGS and In_xS_y. $CuIn_5S_8$ is an n-type semiconductor with a band gap energy of 2.0 eV. It is known to contain a large number of vacancies. Thus, the $CuIn_5S_8$ layer provides a high density of recombination centers. Recombination leads to a decay of the photovoltaic performance of the solar cell. Therefore, for ALD-In_2S_3 as buffer layers for CIGS solar cells, it is detrimental to the solar-cell performance to perform the deposition at substrate temperatures larger than about 210°C-220°C.

A broader overview of structural and chemical investigations of CIGS/ALD-In_2S_3 interfaces can be found in Ref. 4.

References

1. K. Ramanathan, M.A. Contreras, C.L. Perkins, S. Asher, F.S. Hasoon, J. Keane, D. Young, M. Romero, W. Metzger, R. Noufi, J. Ward, A. Duda, Prog. Photovolt.: Res. Appl. **11** (1999) 225.
2. N. Naghavi, S. Spiering, M. Powalla, B. Canava, A. Taisne, J.-F. Guillemoles, S. Taunier, A. Etcheberry, D. Lincot, in: "Compound Semiconductor Photovoltaics", Eds. R. Noufi, C. Cahen, W. Shafarman, L. Stolt, Mat. Res. Soc. Symp. Proc. Vol. 763, MRS, Warrendale, PA, USA, 2003, p. B9.9.1.
3. A. Strohm, L. Eisenmann, R.K. Gebhardt, A. Harding, T. Schlötzer, D. Abou-Ras, H.W. Schock, to be published in Thin Solid Films.
4. D. Abou-Ras, H. Heinrich, G. Kostorz, M. Powalla, S. Spiering, A.N. Tiwari, in: "Proceedings of the 19th European Photovoltaic Solar Energy Conference and Exhibition, Paris, France, June 7–11, 2004", no Eds., WIP Munich and ETA Florence, 2004, p. 1772.

Research at the Electron Microscopy Center (EMEZ)

5. Atomic force microscopy of biological material embedded in epoxy resin

Contacts: Dr. N. Matsko
Dr. M. Müller

Our current understanding of the cellular ultrastructure is largely derived from the analysis of thin sections of resin-embedded biological material by transmission electron microscopy (TEM). The appearance of the ultrastructural elements varies with the applied protocol (buffers, chemical fixation and dehydration or cryofixation followed by freeze substitution, type of embedding resin). Depending on the quality of preservation, the interaction of the structures with the embedding resin may change and will finally result in a different copolymerization of biological and resin macromolecules. Different interactions of resin molecules with bio-

macromolecules is assumed to result in local variations of the mechanical properties of the polymerized material, e.g., the stiffness of membranes could vary according to the protein content, or an embedded protein filament would show a different stiffness than the pure embedded resin. Atomic-force microscopy (AFM) analysis in tapping-mode phase contrast appears to be the method of choice to assess such variations of stiffness and other mechanical properties.

Basic considerations of the process of ultrathin sectioning [1] indicate that most section artifacts (compression, chatter, knife marks) are, with the exception of the knife marks, mainly expressed in the ultrathin section and not in the block face which, therefore, can be extremely flat and may display the „real" dimensions.

In this project**,** biological samples (nematodes) were high pressure frozen, subsequently freeze substituted in acetone containing 2% of OsO_4 and embedded in epon/araldite resin (Hohenberg et al. 1994 [2]). Ultrathin sections (obtained with the help of a diamond knife) and the block face were mounted on appropriate supports for TEM and AFM. Prior to AFM analysis, the block faces were washed with ethanol to remove plastisizer, non crosslinked resin and other molecules of the embedding mixture. A Nano Scope III (DI, USA) equipped with a J scanner and silicon nitride cantilevers (force constant 10 N/m, tip radius 10 nm) was used in tapping mode [3].

The results indicate that most ultrastructural details known from TEM of thin sections can also be visualized by AFM of block faces by topographic and/or stiffness contrast. Unlike TEM, no additional treatment for contrast enhancement like heavy-metal staining is required. On the block face of pure epoxy resin, very little topographic contrast is observed and phase contrast reveals a very homogeneous stiffness (Fig. 5.1).

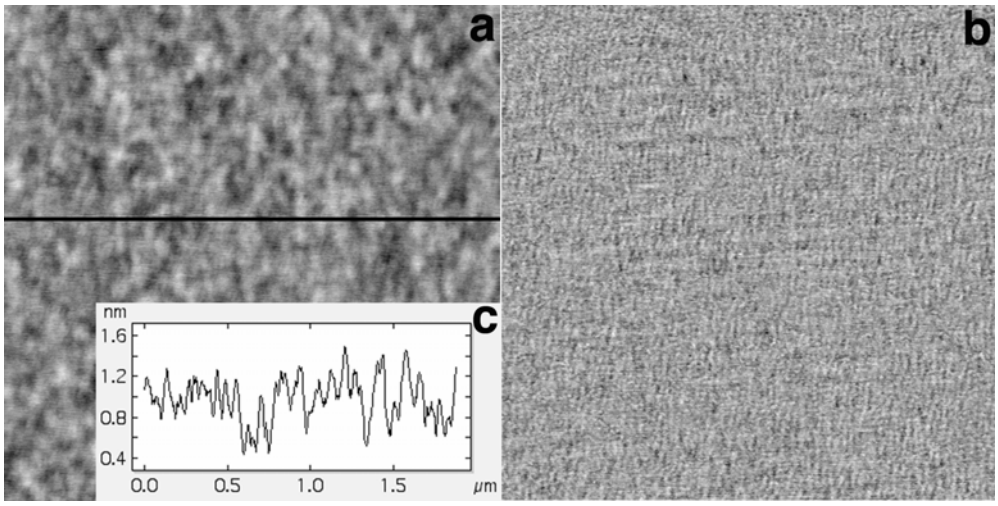

Fig. 5.1 AFM (a) height and (b) phase images recorded in tapping mode on the block face of the pure epoxy resin after microtomy. Image width is 2 µm The contrast covers height variations of 0-3 nm and phase variations of 0-3°. (c) Cross-sectional profile across an arbitrarily selected position in (a).

Where the section proceeds through the biological material (Fig. 5.2), the block face shows significant topographic contrast, which seems to depend on the nature of the embedded material. The viscosity of the various components of the resin formulation determines the quality of impregnation of the different biological structures and may result in local variations of the

initial resin formulation depending on the permeability (porosity) of the cellular constituents. These local variations of the resin formulation may additionally be influenced by the interaction of the highly reactive epoxy group with the biological material (free amino and carboxy groups of proteins) [4]. Thus, the resin-embedded and polymerized biological material will have a locally variable hardness and a locally variable amount of non-cross-linked resin and other molecules of the embedding cocktail, which, after removal by ethanol, may reflect the spatial distribution of the biological constituents. The different interaction of the biological constituents with the embedding resin in AFM is best visualized by phase contrast using a hard tapping mode which reflects the stiffness variation of the examined surface. These tuning parameters ensure that the phase-shift data will be expressed in a predictable manner in the micrographs where dark regions (low phase-shift) are softer while lighter regions (larger phase shift) are harder.

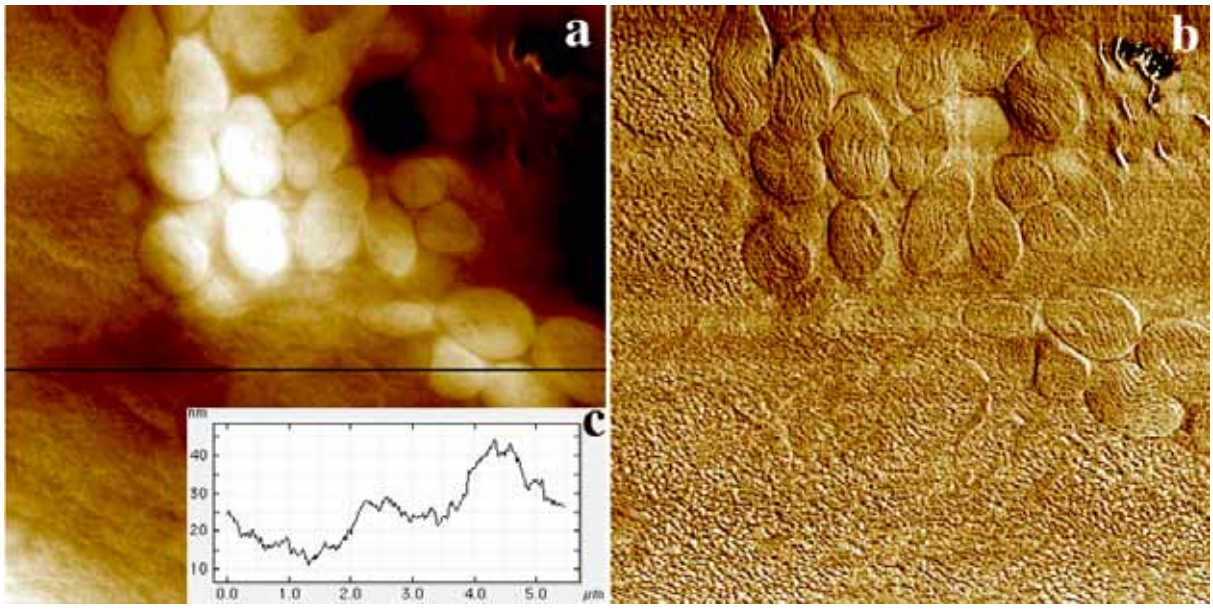

Fig. 5.2 AFM (a) height and (b) phase images recorded in tapping mode on the block face of an embedded mite after microtomy. Image width is 6 µm. The contrast due to height variations is 0-45 nm, and phase variations are 0-3°. (c) Cross-sectional profile across an arbitrarily selected position in (a).

The experimental setup described above is suitable for the simultaneous examination of the block face by AFM and the corresponding thin section by TEM. In TEM, the ultrastructure is visualized by staining with heavy metals, but only the structures that react with the staining agents and that can be reached by the staining agents are detected. Furthermore, the two-dimensional TEM image represents a projection (superposition) of all sufficiently scattering structures from a 50 to 90 nm thick volume (Fig. 5.3c). Thus, cell organelles, membranes, protein filaments, nucleic acids are clearly detected but, e.g., many proteins in the cytoplasm of the cell remain invisible.

AFM, on the contrary, images the very surface of the cut block (Fig. 5.3b). Instead of heavy-metal-stained structures, it uses height and/or stiffness variations that depend on the interaction of the epoxy resin with the ultrastructural components. Therefore, we cannot expect that AFM provides structural information identical to TEM, but similar and new ultrastructural aspects may be revealed.

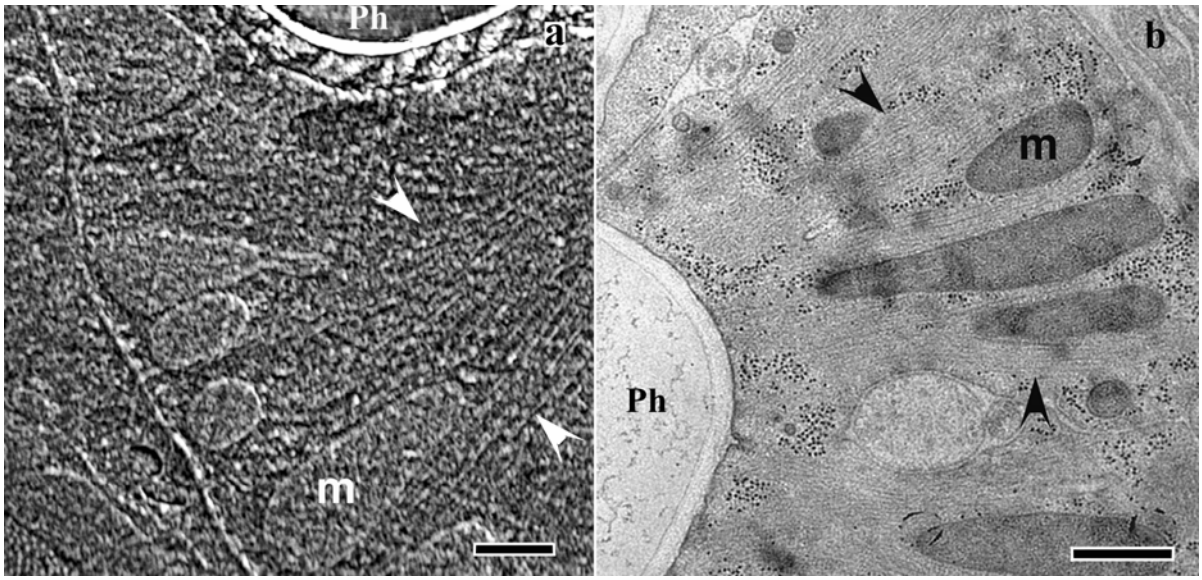

Fig. 5.3 (a) AFM phase image of the block face surface and (b) TEM image of an ultrathin section from the nematode C. elegans embedded in soft epoxy resin. AFM and TEM images of a similar area of the same nematode are compared. Amplitude variation: 0-50 nm; phase variation: 0-5°. Scale bars correspond to 500 nm. Arrows point to actin filaments, **m** mitochondria, **Ph** pharynx

In conclusion, AFM can be developed into a tool to extract ultrastructural information from the interior of cells and tissues. Initial data suggest a resolution close to TEM of thin sections, and the information to be complementary.

References

1. J.-C. Jesior, J. Ultrastruct. Molec. Res**. 95** (1986) 210.
2. H. Hohenberg, K. Mannweiler, M. Mueller, Journal of Microscopy **175** (1994) 34.
3. S. Magonov, D. Reneker, Annu. Rev. Mater. Sci. **27** (1997) 175.
4. B.E. Causton, in: "The Science of Biological specimen preparation for microscopy and microanalysis", Eds. M. Mueller, R.P. Becker, A. Boyde, J.J. Wolosewick, Scanning Electron Microscopy inc., AMF O'Hare, 1986, p.209.

INSTITUTE OF APPLIED PHYSICS ETH ZÜRICH

Available Facilities

The scientific and technical staff of the institute continue to construct or modify most of the in-house instruments according to special requirements and new technological developments. At the institute, various alloys and single crystals of materials with widely different properties such as melting temperature, ductility and reactivity are produced. For single crystals, high standards of purity, homogeneity and crystal perfection must be fulfilled to satisfy the experimental requirements. Methods for the preparation of crystals and their surfaces are steadily improved.

An experimental setup for electro-chemical phase separation to produce nano-particles from metallic alloys was established. It consists of a simple electrolytic cell with the sample as the anode and a platinum cathode connected to a variable voltage (-30 to +30 V with maximum current of 1 A) potentiometer. A PC-based software control of the potential source serves to record current density versus potential curves during the electrochemical dissolution. Ultrasonic vibration is used to separate and collect nano-particles from the specimen surface.

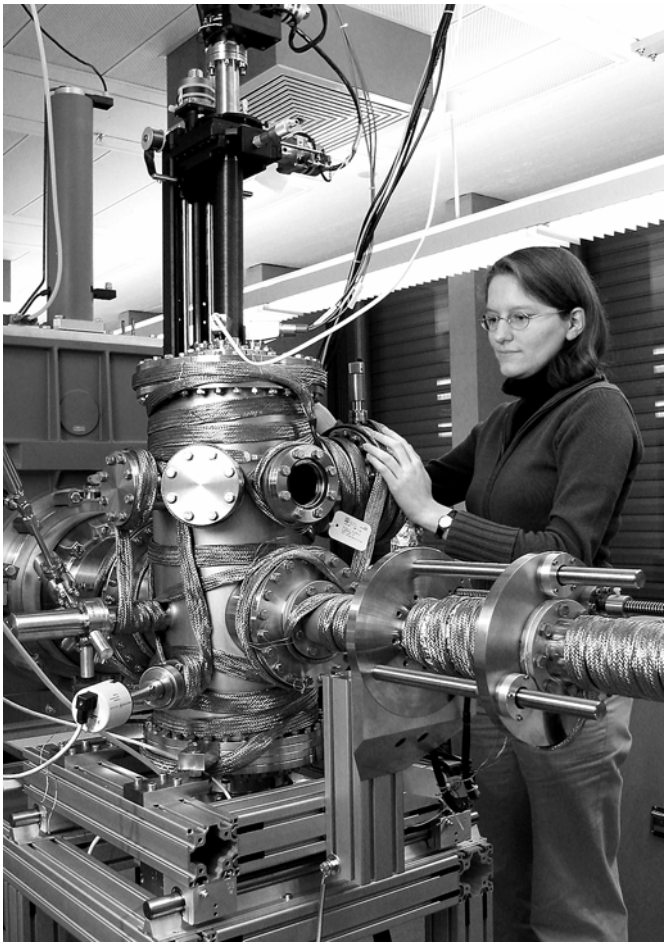

In 2004 further developments were made for near-surface microstructural studies. An AES-LEED unit was added to the UHV chamber to further characterize surfaces prior to diffraction experiments.

The following instruments are available for teaching and research. Renewal programmes are continuing.

Alloy production
- Vacuum induction furnace for melting and casting (20 kW, 10 kHz)
- Arc melting furnace for sets of samples
- Arc melting furnace with casting facility
- Cold-crucible levitation furnace for melting and casting

Crystal growth facilities
- Bridgman furnace
- Bridgman apparatus with quench facility
- Czochralski furnace
- Strain annealing facilities
- High-vacuum electron-beam zone melting apparatus (10 kV, 0.5 A)
- High-frequency zone melting furnace (50 kW, 350 kHz) providing a pressure-controlled inert gas atmosphere

Heat treatment
- Several furnaces for heat treatment from room temperature to 2000°C in vacuum and inert gas atmosphere
- Furnaces for quenching in an inert gas atmosphere or vacuum up to 1500°C

Sample preparation and characterization
- Diamond-bladed disk cutter
- Wire saw
- Butt welding facility
- Metallography laboratory for mechanical, chemical and electrochemical sample preparation
- Setup for flat-surface polishing
- Optical microscopes and an optical interference microscope
- Energy dispersive X-ray fluorescence analysis apparatus
- X-ray facility for Laue and Debye-Scherrer methods
- Differential scanning calorimeter (DSC)
- Ultrasonic device for measurement of elastic constants (pulse-echo overlap method)
- Vickers hardness testing apparatus
- Apparatus to measure electrical resistivity at low and high temperatures
- Spark erosion facility

Mechanical testing
- Two static mechanical testing machines (20 kN, 100 kN, digitally controlled)
- Hydraulic testing machine (± 20 kN)
- Two high-temperature chambers for plastic deformation up to 1200°C
- Variable-field magnetic system for magneto-mechanical testing
- High-temperature testing stage (10 kN) for use in a scanning electron microscope
- Magneto-mechanical testing device for dynamical experiments

Scattering methods
- Two four-circle X-ray diffractometers with high-temperature chamber and an energy-dispersive detector

- High-resolution X-ray diffractometer with a high-temperature chamber and a linear detector for the measurement of scattering profiles
- Kratky chamber for small-angle X-ray scattering in line focus with a linear position-sensitive detector
- Small-angle X-ray scattering facility with point focus and two-dimensional position-sensitive detector (18 kW)
- High-temperature cell for small-angle neutron scattering (jointly with Paul Scherrer Institut)
- Sample chamber for grazing-incidence diffraction.

Computing
Servers (3), personal computers (33), for control of experiments, data acquisition, model calculations.

Facilities at the Electron Microscopy Center

- Facilities for the preparation of samples for transmission and scanning electron microscopy:
  - dimple grinder, facilities for vapor deposition, ion-beam sputtering, plasma cleaning, electropolishing
  - high-pressure freezing, jet freezing, plunge freezing, freeze-substitution, critical-point drying, freeze-fracturing and freeze-drying, shadowing and sputter coating, sectioning and labelling

- Scanning electron microscopes (SEMs)
  - 40 kV SEM, EDX, OIM
  - 30 kV SEM, FEG, SE and BS detectors
  - 30 kV high resolution SEM, FEG , SE and BS detectors, cryoholder
  - 30 kV ESEM, SE and BS detectors

- Transmission electron microscopes (TEMs)
  - 100 kV TEM for routine microscopy, 2 CCD cameras
  - 120 kV routine and cryo TEM, attached cryo-preparation chamber, CCD camera
  - 120 kV routine and cryo TEM, in-column energy filter, CCD camera
  - 200 kV cryo TEM, FEG, post-column energy filter
  - 300 kV high-resolution TEM, STEM, EDX, CBED, CCD camera
  - 300 kV high-resolution TEM, FEG, post-column energy filter (EFTEM, EELS), EDX, HAADF (Z contrast imaging in STEM mode), CCD camera

- Imaging plates with scanner

INSTITUTE OF APPLIED PHYSICS ETH ZÜRICH

External oral and poster presentations by members of the institute 2004

(for multi-author presentations, the name of the speaker is underlined)

D. Abou-Ras, G. Kostorz, A. Romeo[1], D. Rudmann[1], A.N. Tiwari[1]
"Structural and chemical investigations of CBD- and PVD-CdS buffer layers and interfaces in Cu(In,Ga)Se_2-based thin film solar cells"
E-MRS 2004 Spring Meeting, Strasbourg, France, 25 May 2004 (Poster).

D. Abou-Ras, G. Kostorz, D. Bremaud[1], M. Kälin[1], F.V. Kurdesau[1], A.N. Tiwari[1], M. Döbeli[2]
"Formation and characterization of $MoSe_2$ in Cu(In,Ga)Se_2-based solar cells"
E-MRS 2004 Spring Meeting, Strasbourg, France, 27 May 2004.

Zs. Geller
"The role of Re in Ni-alloys"
ELTE-ETH Seminar on Materials Science, Héviz, Hungary, 16 September 2004.

F. Krogh
"Plasticity of B2 RuAl"
ELTE-ETH Seminar on Materials Science, Héviz, Hungary, 16 September 2004.

G. Kostorz
"Microstructure of alloys from neutron scattering"
Kolloquium Max-Planck-Institut für Eisenforschung GmbH, Düsseldorf, Germany, 20 April 2004.

G. Kostorz
"Magnetoplasticity"
ELTE-ETH Seminar on Materials Science, Héviz, Hungary, 16 September 2004.

P. Müllner[3]
"Magnetoplastizität: Schlüssel zu neuen Sensoren und Aktuatoren"
Metal Physics Colloquium, Montanistic University Leoben, Austria, 26 January 2004.

D. Mukherji
"Nanostructures from two-phase Ni-base alloys"
ELTE-ETH Seminar on Materials Science, Héviz, Hungary, 18 September 2004.

---

[1] Laboratory for Solid State Physics, Thin Film Physics Group, ETH Zürich
[2] Paul Scherrer Institute, Villigen-PSI, Switzerland
[3] now at: Boise State University, Boise, ID, USA

D. Mukherji, R. Gilles[1], P. Strunz[2], J. Rösler[3], G. Kostorz
"Characterization of nano-particles of nickel aluminides and silicides"
8th International Conference on Nanometer Scale Science and Technology, NANO-8, Venice, Italy, 1 July 2004.

D. Mukherji, P. Strunz[2], R. Gilles[1], R. Müller[4], J. Rösler[3], G. Kostorz
"A novel method to produce nano-scale particles from intermetallic phases"
7th International Conference on Nanostructured Materials, Wiesbaden, Germany, 20-24 June 2004 (Poster).

G. Pigozzi, D. Mukherji
"Nanoparticles of Ni_3Al and Ni_3Si obtained from controlled precipitate morphologies in Ni-Al, Ni-Si and Ni-Al-Si alloys"
ELTE-ETH Seminar on Materials Science, Héviz, Hungary, 18 September 2004.

A. Romeo[5], D. Abou-Ras, R. Gysel[5] S. Buzzi[5], D.L. Bätzner[5], D. Rudmann[5], H. Zogg[5], A.N. Tiwari[5]
"Properties of CIGS solar cells developed with evaporated II-VI buffer layers"
14th International Photovoltaic Science and Engineering Conference, Bangkok, Thailand, 29 January 2004.

B. Schönfeld
"Diffuse Streuung in der Legierungsforschung"
Seminar in Materialwissenschaft für Fortgeschrittene, ETH Zürich, 28 June 2004.

B. Schönfeld
"Atomic/magnetic short-range order and static atomic displacements in Cu-Mn"
ELTE-ETH Seminar on Materials Science, Héviz, Hungary, 16 September 2004.

B. Schönfeld
"Diffuse scattering of binary alloys"
Symposium on "Scattering from disordered and defective materials", University of Houston, Houston TX, USA, 2 October 2004.

B. Schönfeld, M.J. Portmann, Ch. Steiner, G. Kostorz, F. Altorfer[2], J. Kohlbrecher[2], A. Mazuelas[6], H. Metzger[6]
"Local order or local decomposition in the solid solutions of Ni-Au and Pt-Rh?"
2004 TMS Annual Meeting, Charlotte NC, USA, 15 March 2004.

A.S. Sologubenko
"Formation of twinned tetragonal ferromagnetic $L1_0$ MnAl-C"
ELTE-ETH Seminar on Materials Science, Héviz, Hungary, 16 September 2004.

[1] Technical University Munich, Garching, Germany
[2] Paul Scherrer Institute, Villigen-PSI, Switzerland
[3] Technical University Braunschweig, Braunschweig, Germany
[4] Institute of Physical Hightechnology, Jena, Germany
[5] Laboratory for Solid State Physics, Thin Film Physics Group, ETH Zürich
[6] ESRF, Grenoble, France

A.S. Sologubenko, H. Heinrich[1], P. Müllner[2], G. Kostorz
"Bulk formation of plate-like tetragonal tau phase in MnAl-C alloys"
MRS 2004 Fall Meeting, Boston, USA, 30 November 2004 (Poster).

A.S. Sologubenko, P. Müllner[2], H. Heinrich[1], G. Kostorz
"Formation of twinned tetragonal ferromagnetic $L1_0$ MnAl-C"
Workshop on "Intelligent Shape Memory and Magnetoplastic Materials, ISMEM 2004", Niedzica, Poland, 12 October 2004.

Ch. Steiner
"Near-surface order of Pt-Rh"
ELTE-ETH Seminar on Materials Science, Héviz, Hungary, 18 September 2004.

Ch. Steiner, M.M.I.P. van der Klis, B. Schönfeld, G. Kostorz, B. Patterson[3], P. Willmott[3]
"Bulk and near-surface microstructure of Pt-Rh"
Junior Euromat 2004, Lausanne, Switzerland, 6-9 September 2004 (Poster).

A. Strohm[4], L. Eisenmann[4], R.K. Gebhardt[4], A. Harding[4], T. Schlötzer[4], D. Abou-Ras, H.W. Schock[4]
"ZnO/In_xS_y/Cu(In,Ga)Se_2 solar cells fabricated by coherent heterojunction formation"
E-MRS 2004 Spring Meeting, Strasbourg, France, 25 May 2004.

M.M.I.P. van der Klis
"Why grazing incidence diffraction on Ag-Mn?"
ELTE-ETH Seminar on Materials Science, Héviz, Hungary, 16 September 2004.

External oral and poster presentations by EMEZ staff

H. Gross
"10 Jahre digitale Bilderfassung in der Elektronenmikroskopie der ETH Zürich"
Workshop ETH Zürich, 9 November 2004.

A. Käch
"Beschichtungstechniken für die Elektronenmikroskopie"
Seminar der Technischen Akademie Esslingen on "Rasterelektronenmikroskopie und Analyse von Mikrobereichen und Oberflächenschichten", Sarnen, Switzerland, 13 Mai 2004.

A. Käch
"High pressure freezing and freeze fracturing"
Söderberg Symposium Lund on Emerging Technologies in Biomedical Research, Lund, Sweden, 25 May 2004.

[1] University of Central Florida, Orlando, FL, USA
[2] now at: Boise State University, Boise, ID, USA
[3] Paul Scherrer Institute, Villigen-PSI, Switzerland
[4] University of Stuttgart, Stuttgart, Germany

A. Käch
"High pressure freezing and freeze fracturing"
Third International Cryo EM Workshop, University of British Columbia, Vancouver, Canada, 16 June 2004.

A. Käch
"High pressure freezing"
CEMOVIS (Cryo electron microscopy of vitreous sections), University of Lausanne, Lausanne, Switzerland, 28 June 2004.

A. Käch
"High pressure freezing"
EMBO/FEBS Practical Course: "Electron microscopy and stereology in cell biology", Institut Pasteur, Paris, France, 15 September 2004.

M. Müller, N. Matsko
"High pressure freezing: an overview"
16th International Congress of the International Federation of Associations of Anatomists, Kyoto, Japan, 26 August 2004.

N. Matsko, M. Müller
"AFM of biological material embedded in epoxy resin"
13th European Microscopy Congress (EMC 2004), Antwerp, Belgium, 26 August 2004.

M. Müller
"Theory and praxis of high pressure freezing"
Seminar Toyama University, Toyama, Japan, 28 August 2004

M. Müller
"Evaluation of high pressure frozen biological samples by transmission- and scanning-electron microscopy and atomic force microscopy"
Seminar Japan Women's University, Tokyo, Japan, 30 August 2004.

M. Müller, N. Matsko
"Cellular ultrastructure by atomic force microscopy"
16th International Congress of the International Federation of Associations of Anatomists, Kyoto, Japan, 25 August 2004.

M. Müller, P. Walther[1]
"High resolution scanning electron microscopy in biology"
16th International Congress of the International Federation of Associations of Anatomists, Kyoto, Japan, 23 August 2004.

R. Wepf[2], T. Richter[2], M. Sattler[2], A. Käch
"Improvements for HR- and Cryo-SEM by the VCT 100 high-vacuum cryo transfer system and SEM cooling stage"
Microscopy & Microanalysis 2004, Savannah, Georgia, USA, 2-6 August 2004 (Poster).

[1] University of Ulm, Ulm, Germany
[2] R&D Beiersdorf AG, Hamburg

R. Wepf[1], T. Richter[1], M. Sattler[1], A. Käch
"Improvements for HR- and Cryo-SEM by the VCT 100 high-vacuum cryo transfer system and SEM cooling stage"
13th European Microscopy Congress (EMC 2004), Antwerp, Belgium, 22-27 August 2004 (Poster).

R. Wepf[1], T. Richter[1], M. Sattler[1], A. Käch
"Improvements for HR- and Cryo-SEM by the VCT 100 high-vacuum cryo transfer system and SEM cooling stage"
Réunion: "Cryométhodes en Microscopie Electronique et Systèmes Moléculaires Organisés", Université Paris-Sud, Orsay, France, 13-14 December 2004 (Poster).

[1] R&D Beiersdorf AG, Hamburg

INSTITUTE OF APPLIED PHYSICS ETH ZÜRICH

Publications of members of the institute, 2004

GK 259
D. Abou-Ras, H. Heinrich[1], G. Kostorz, M. Powalla[2], S. Spiering[2], A.N. Tiwari[3]
"Structural and chemical investigations of interfaces between Cu(In,Ga)Se_2 and atomic layer deposited In_2S_3"
in Proceedings of the 19th Photovoltaic Solar Energy Conference, 7-11 June 2004, Paris, France (no Eds.), WIP-Munich/ETA-Florence 2004, pp. 1772-1775.

GK 255
V.A. Chernenko[4], V.A. L'vov[5], P. Müllner[6], G. Kostorz, T. Takagi[7]
"Magnetic-field-induced superelasticity of ferromagnetic thermoelastic martensites: Experiment and modeling"
Phys. Rev. B **69** (2004) 134410-1 – 134410-8.

APK 91
K. Durose[8], S.E. Asher[9], W. Jaegermann[10], D. Levi[9], B.E. McCandless[11], W. Metzger[9], H. Moutinho[9], P.D. Paulson[11], C.L. Perkins[9], J.R. Sites[12], G. Teeter[9], M. Terheggen
"Physical characterization of thin-film solar cells"
Prog. Photovolt: Res. Appl. **12** (2004) 177-217.

GK 251
G. Kostorz
"Microstructural studies of alloys"
in "Applied Crystallography" H. Morawiec, D. Stróz, Eds., World Scientific Publishing Co. Pte, Ltd., Singapore, 2004, pp. 199-204.

GK 258
L. Lityńska[13], J. Dutkiewicz[13], H. Heinrich[14], G. Kostorz
"Structure of precipitates in Al-Mg-Si-Sc and Al-Mg-Si-Sc-Zr alloys"
Acta Metallurgica Slovaca **10** (2004) 514-519.

---

[1] University of Central Florida, Orlando, FL, USA
[2] Zentrum für Sonnenenergie- und Wasserstoffforschung, Stuttgart, Germany
[3] Laboratory for Solid State Physics, Thin Film Physics Group, ETH Zürich
[4] Institute of Magnetism, Kyiv, Ukraine
[5] Taras Shevchenko University, Kyiv, Ukraine
[6] now at: Boise State University, Boise, ID, USA
[7] Tohoku University, Sendai, Japan
[8] University of Durham, UK
[9] National Renewable Energy Laboratory, Golden, CO, USA
[10] Darmstadt University of Technology, Darmstadt, Germany
[11] University of Delaware, Newark, DE, USA
[12] Colorado State University, Fort Collins, CO, USA
[13] Polish Academy of Sciences, Kraków, Poland
[14] University of Central Florida, Orlando, FL, USA

APK 93
M. Maučec[1], R.J. de Meijer[1], M.M.I.P. van der Klis, P.H.G.M. Hendriks[1], D.G. Jones[2]
"Detection of radioactive particles offshore by γ-ray spectrometry Part II: Monte Carlo assessment of acquisition times"
Nucl. Instr. and Meth. A **525** (2004) 610-622.

GK 249
P. Müllner[3], V.A. Chernenko[4], G. Kostorz
"Large cyclic magnetic-field-induced deformation in orthorhombic (14*M*) Ni-Mn-Ga martensite"
J. Appl. Phys. **95** (2004) 1531-1536.

GK 252
P. Müllner[3], V.A. Chernenko[4], D. Mukherji, G. Kostorz
"Cyclic magnetic-field-induced deformation and magneto-mechanical fatigue of Ni-Mn-Ga ferromagnetic martensites"
in "Materials and Devices for Smart Systems", Y. Furuya, E. Quandt, Q. Zhang, K. Inoue, M. Shahinpoor, Eds., Mat.Res.Soc.Symp.Proc. Vol. 785, MRS, Warrendale, PA, USA, 2004, pp. 415-420.

GK 250
D. Mukherji, R. Müller[5], R. Gilles[6], P. Strunz[7], J. Rösler[8], G. Kostorz
"Nanocrystalline Ni_3Al-type intermetallic phase powder from Ni-base superalloys"
Nanotechnology **15** (2004) 648-657.

GK 260
P. Müllner[3], V.A. Chernenko[4], G. Kostorz
"Large magnetic-field-induced deformation and magneto-mechanical fatigue of ferromagnetic Ni-Mn-Ga martensites"
Mater. Sci. Eng. A **387-389** (2004) 965-968.

GK 256
M.J. Portmann, R. Erni[9], H. Heinrich[10], G. Kostorz
"Bulk interfaces in a Ni-rich Ni-Au alloy investigated by high-resolution Z-contrast imaging"
Micron **35** (2004) 695-700.

[1] Rijksuniversiteit Groningen, Groningen, The Netherlands
[2] British Geological Survey, Nottingham, UK
[3] now at: Boise State University, Boise, ID, USA
[4] Institute of Magnetism, Kyiv, Ukraine
[5] Institute for Physical Hightechnology, Jena, Germany
[6] Technical University Munich, Garching, Germany
[7] Paul Scherrer Institute, Villigen-PSI, Switzerland
[8] Technical University Braunschweig, Braunschweig, Germany
[9] University of California-Davis, CA, USA
[10] University of Central Florida, Orlando, FL, USA

APK 94
J. Rösler[1], O. Näth[1], F. Schmitz[1], D. Mukherji
"Design of nanoporous superalloy membranes by self-assembly of the γ'-phase"
in "Proc. Superalloys 2004", K.A. Green, T.M. Pollock, H. Harada, T.E. Howson, R.C. Reed, J.J. Schirra, S. Walston, Eds., TMS, Warrendale, PA, USA, 2004, pp. 501-506.

APK 92
A. Romeo[2], M. Terheggen, D. Abou-Ras, D.L. Bätzner[3], F.-J. Haug[3], M. Kälin[3], D. Rudmann[3], A.N. Tiwari[3]
"Development of thin-film Cu(In,Ga)Se_2 and CdTe solar cells"
Prog. Photovolt: Res. Appl. **12** (2004) 93-111.

GK 257
B. Schönfeld, R. Bucher[4], G. Kostorz, M. Zolliker[5]
"Magnetic and atomic short-range order in Cu-rich Cu-Mn"
Phys. Rev. B **69** (2004) 224205-1 – 224205-9.

APK 95
C. Siemers[1], M. Bäcker[1], D. Mukherji, J. Rösler[1]
"Microstructure evolution in shear bands during the chip formation of Ti6Al4V"
in "Proc. of Ti-2003 Science and Technology",vol. 2, G. Luetjering, J. Albrecht, Eds., Wiley-VCH, Weinheim, Germany, 2004, pp. 839-846.

GK 253
A.S. Sologubenko, P. Müllner[6], H. Heinrich[7], G. Kostorz
"On the plate-like τ-phase formation in MnAl-C alloys"
Z. Metallkd. **95** (2004) 486-491.

GK 254
M. Terheggen, H. Heinrich[7], G. Kostorz, D. Baetzner[3], A. Romeo[2], A.N. Tiwari[3]
"Analysis of bulk and interface phenomena in CdTe/CdS thin-film solar cells"
Interface Science **12** (2004) 259-266.

GK 248
S.Y. Yu[8], B. Schönfeld, H. Heinrich[7], G. Kostorz
"Short-range order in h.c.p. Ag-Al"
Progr. Mater. Sci. **49** (2004) 561-579.

[1] Technical University, Braunschweig, Braunschweig, Germany
[2] University of Verona, Verona, Italy
[3] Laboratory for Solid State Physics, Thin Film Physics Group, ETH Zürich
[4] University of Cape Town, Rondebosch, South Africa
[5] Paul Scherrer Institute, Villigen-PSI, Switzerland
[6] now at: Boise State University, Boise, ID, USA
[7] University of Central Florida, Orlando, FL, USA
[8] ESEC SA, Cham, Switzerland

Publications of EMEZ staff

EM 5
H. Eberl,[1] P. Tittmann, R. Glockshuber[1]
"Characterization of recombinant, membrane-attached full-length prion protein"
J. Biol. Chem. **279** (2004) 25058-25065.

EM 1
N. Matsko, M. Müller
"AFM of biological material embedded in epoxy resin"
J. Structural Biology **146** (2004) 334-343.

EM 3
A. Napoli[2], M. Valentini[2], N. Tirelli[2], M. Mueller, J. A. Hubbell[2]
"Oxidation-responsive polymeric vesicles"
Nature Materials **3** (2004) 183-189.

EM 4
R.A. Santarella[3], G. Skinotis[3], K.N. Goldie[3], P. Tittmann, H. Gross, E.M. Mandelkow[4], E. Mandelkow[4], A. Hoenger[3]
"Surface-decoration of microtubules by human tau"
J. Mol. Biol. **339** (2004) 539-553.

EM 2
H.M. Wyss[5], E. Tervoort[5], L.P. Meier[5], M. Müller, L. Gauckler[5]
"Relation between microstructure and mechanical behaviour of concentrated silica gels"
J. Colloid and Interface Science **273** (2004) 455-462.

Doctoral Theses 2004

D. Rudmann (Dr. sc. ETH Zürich)
"Effects of sodium on growth and properties of $Cu(In,Ga)Se_2$ thin films and solar cells"

D. Zimin (Dr. sc. nat.)
"Growth and properties of optoelectronic structures based on IV-VI materials"

[1] Institute of Molecular Biology and Biophysics, ETH Zürich
[2] Institute for Biomedical Engineering, ETH Zürich
[3] European Molecular Biology Laboratory, Heidelberg, Germany
[4] Max Planck Unit for Molecular Biology c/o DESY Hamburg, Hamburg, Germany
[5] Nonmetallic Materials, ETH Zürich